ACS APPLIED MATERIALS & INTERFACES

www.acsami.org

Research Article

Improved Performance for Thermally Evaporated Perovskite Light-Emitting Devices via Defect Passivation and Carrier Regulation

Kuifeng Jia, Li Song,* Yongsheng Hu, Xiaoyang Guo, Xingyuan Liu,* Chong Geng, Shu Xu, Ruiting Fan, Lixin Huang, Nannan Luan, and Wengang Bi*

Cite This: *ACS Appl. Mater. Interfaces* 2020, 12, 15928−15933

Read Online

ACCESS | Metrics & More | Article Recommendations | Supporting Information

ABSTRACT: Efficient inorganic perovskite light-emitting devices (PeLEDs) with a vacuum-deposited $CsPbBr_3$ emission layer were realized by introducing an ultrathin 2-phenylethanamine bromide interlayer. The PEA^+ cations not only passivated the nonradiative defects by terminating on the $CsPbBr_3$ surface but also regulated the charge transport to balance the hole and electron transport. Consequently, the PeLEDs exhibit significantly promoted performance with a turn-on voltage of 3 V, a maximum current efficiency of 14.64 cd A^{-1}, and an external quantum efficiency of 4.10%. Our work would provide instructive guidance for realizing efficient PeLEDs based on a vacuum processing method via focusing on the interface modification between the perovskite layer and the carrier transport layer.

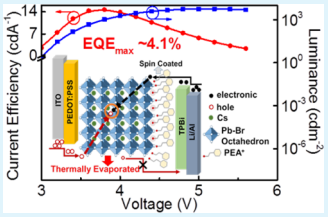

KEYWORDS: *all-inorganic perovskite, interfacial modification, light-emitting, thermal evaporation, charge transport*

INTRODUCTION

In recent years, by virtue of the excellent optical and electrical properties such as high carrier mobility, long carrier diffusion length, high photoluminescence quantum efficiency, high absorption coefficient, tunable energy band gap, high color purity, and so on,[1−5] metal halide perovskite materials are emerging as promising materials and have received intensive investigation in the fields of optoelectronics including solar cells,[6,7] photodetectors,[8,9] field effect transistors,[10] and light emitting diodes.[11,12]

Since the first organic−inorganic hybrid perovskite light-emitting device (PeLED) based on $CH_3NH_3PbBr_3$ perovskite was reported in 2014,[13] PeLEDs have developed rapidly in the past few years with an external quantum efficiency (EQE) exceeding 20%.[14−16] Among them, the all-inorganic perovskite $CsPbX_3$ (X = Cl/Br/I) exhibits superior thermal and moisture stability in contrast to the organic−inorganic hybrid perovskite.[17,18] So far, most of the reported devices are solution processed, which is easily limited by the solubility of the material in organic solvents, especially for the $CsPbX_3$ compounds that suffer from low solubility.[19,20] Fortunately, thermal evaporation emerged as an intelligent strategy to prepare high quality perovskites without considering the solubility limitation.[21,22] Moreover, the thermal evaporation method enables high reproducibility and reliability because of the well-controlled vacuum preparation condition as well as compatibility with mature fabrication facilities for organic light-emitting devices.[23] This strategy has been successfully demonstrated in developing perovskite solar cells with power conversion efficiency up to 20%, comparable to solution-processed devices.[24−27]

However, there are only few reports on thermally evaporated PeLEDs, and their performance is still lagging behind that of the solution-processed counterparts.[23,28,29] Hu et al. cautiously adjusted the coevaporation ratio of CsBr and $PbBr_2$ in the prepared all-inorganic green PeLED and achieved an EQE of 1.55% as well as a maximum luminance of 5765 cd m^{-2}.[28] A low photoluminescence quantum yield (PLQY) of ∼12.3% for the thermally deposited emission layer (EML) would be a major reason leading to the inferior performance, indicating that there exists plentiful defects either from the bulk or the interface or both of them. Lian et al. further improved the PLQY of the EML to ∼40% by passivating the bulk defects using the Cs_4PbBr_6 phase and the EQE was promoted to ∼2.5%.[29] Although the Cs_4PbBr_6 can passivate the nonradiative defects, its low conductivity also sacrifices the charge transport resulting in a tradeoff between the PLQY and charge transport, and ultimately limits further improvement of the performance. Thus, it is urgently necessary to exploit alternative strategies to passivate the residual defects effectively. On the other hand, the balanced charge transport also plays a crucial role in determining the device performance. Replacing the PEDOT:PSS, Li et al. employed NiO_x as the hole transport layer to mitigate the interfacial photoluminescence (PL) quenching and regulate the charge transport simultaneously, making the thermally deposited

Received: January 20, 2020
Accepted: March 5, 2020
Published: March 5, 2020

https://dx.doi.org/10.1021/acsami.0c01173
ACS Appl. Mater. Interfaces 2020, 12, 15928−15933

$CsPbBr_3$ PeLED achieve the highest hitherto EQE of 3.26%.[23] Such progress reminds us to focus on passivating the interfacial defects and manipulating the carrier transport to improve the performance of the thermally deposited PeLEDs.

Interfacial engineering would possibly be an effective method to ameliorate the device performance. This intelligent strategy has been broadly investigated in solution-processed optoelectronic devices.[30−34] Among them, bulky ammonium halides that were widely adopted in quasi-2D perovskites can terminate with the corner-sharing Pb−X octahedrons to fill the traps, improve the multiple quantum well structure, and stabilize the desired perovskite phase.[31] Besides, the bulky cations can impede carrier transport because of the insulating properties.[35] Therefore, such materials would be potential interlayers to satisfy the requirements mentioned above. However, its effect and mechanism have not been fully explored in the thermally evaporated PeLEDs.

In this work, aiming at improving the performance of PeLEDs with a thermally evaporated all-inorganic $CsPbBr_3$ EML, interfacial engineering has been developed to both suppress the nonradiative recombination and balance the charge carrier transport. 2-Phenylethanamine bromide (PEABr) was adopted as an ultrathin interlayer between the $CsPbBr_3$ EML and the electron transport layer. PEA^+ can terminate on the $CsPbBr_3$ surface and passivate defects to improve the optical properties of the perovskite films. Meanwhile, the bulky PEA^+ can impede both the holes and the electron transport resulting in a more balanced charge transport and an alleviated charge−exciton interaction. Consequently, the efficiency of the thermally evaporated PeLEDs is significantly improved with a current efficiency of 14.64 cd A^{-1} and an EQE of 4.10% with a narrow electroluminescence spectrum (full width at half maximum (FWHM) of ∼18 nm), demonstrating the plausibility of this effective interfacial engineering strategy. Our results would shed light on rational designs for the high-performance thermally evaporated PeLEDs.

RESULTS AND DISCUSSION

The all-inorganic perovskite EML was prepared by thermally depositing CsBr and $PbBr_2$ pairs alternatively and annealing at 110 °C. Prior to the surface defects passivation, we first optimized the relative amount of CsBr and $PbBr_2$ in each pair to ensure minimum bulk defects in the EML. As demonstrated by the PL spectra in Figure 1a, when the CsBr and $PbBr_2$ thickness ratio reaches 9.8:3.2 (the actual thickness of each layer is 9.8 and 3.2 nm, respectively), the light emission intensity reaches the maximum, indicating the least bulk defects in the EML. The X-ray diffraction (XRD) pattern was measured to explore the crystal structure of the perovskite films. As seen in Figure 1b, the diffraction peaks at 15.2 and 30.7° correspond to the (100) and (200) planes of the $CsPbBr_3$ crystal, respectively (refer to the standard $CsPbBr_3$ XRD card in Figure S1a). The diffraction peaks at 12.7, 20.2, 22.5, 25.5, and 28.7° indicate that the perovskite film contains the Cs_4PbBr_6 phase,[36] which can also be well-verified by the absorption peak at ∼313 nm that corresponds to the band gap energy of Cs_4PbBr_6 (see Figure S1b). The slightly blue-shifted spectra, as the amount of CsBr increases (see Figures 1a and S1c), may be ascribed to the increased Cs_4PbBr_6 phase, which may constrain the crystal size of $CsPbBr_3$.[36] Moreover, the broad reflections of the XRD for the $CsPbBr_3$ phase also indicate the strong constraint by Cs_4PbBr_6. The large band gap of Cs_4PbBr_6 can passivate the defects existed at the $CsPbBr_3$ grain boundaries and thus reduces the nonradiative recombination of photogenerated carriers, leading to the increased PL emission as the CsBr/$PbBr_2$ ratio increases. Further increase in the CsBr/$PbBr_2$ thickness ratio to 11.4:3.2 will result in a slight decrease in the PL intensity. In addition, the multilayer PeLED (see Figure S2a) fabricated with the EML using a CsBr/$PbBr_2$ thickness ratio of 9.8:3.2 also presents the best overall optoelectronic performance, as shown in Figure S2b,c and Table S1. The device exhibits the lowest turn-on voltage of 3 V, a maximum luminance of 8662 cd m^{-2}, a maximum current efficiency of 4.52 cd A^{-1}, and a corresponding EQE of 1.27% that is comparable to the performance reported in the literature where PEDOT:PSS was used as the hole transport layer.[23]

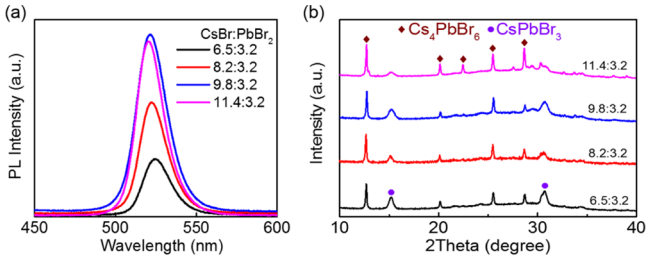

Figure 1. (a) PL curves, and (b) XRD patterns with different thickness ratio of CsBr to $PbBr_2$.

Keeping in mind that the bulk defects of the perovskite EML have been efficiently suppressed, we further used PEABr as the interlayer to passivate the interfacial defects. Considering the insulating properties of the PEABr, which means having too much would deteriorate the electrical performance (discussed below), we carefully controlled the interfacial treatment by using a low concentration of PEABr (1, 2, or 2.5 mg mL^{-1}). Because the morphology of the perovskite film plays a critical role in determining the performance of PeLEDs,[37] atomic force microscopy (AFM) was used to explore the effects of different concentrations of PEABr on the morphology of the perovskite films. It can be seen from Figure 2a−d that the neat perovskite film has a large roughness with a root mean square (RMS) of 8.8 nm. After modification with different concentrations of PEABr, the morphology of the perovskite thin films has been significantly improved. The RMS corresponding to 1 and 2 mg mL^{-1} PEABr decreased to 6.81 and 6.89 nm, respectively. However, when the concentration of PEABr increased to 2.5 mg mL^{-1}, because of excessive PEABr stack, the RMS conversely increased to 7.63 nm. It is anticipated that a smoother film morphology would be beneficial to enable the conformal deposition of overlying layers and improve the photoelectric performance of the PeLEDs. There exists almost no difference in the XRD patterns (see Figure S3) for the PEABr-treated EMLs, demonstrating that the introduction of a small amount of PEABr may not change the crystal structure of the perovskite films.

As shown in Figure 3a, all the perovskite films presented a sharp emission located at the edge of the absorption band because of the intrinsic nature of the direct band gap semiconductor with a peak center at 522 nm and a narrow FWHM of 21 nm. Notably, as the PEABr concentration increased, the PL intensity of the perovskite films gradually enhanced and reached the strongest at a concentration of 2 mg mL^{-1}, demonstrating that the introduction of PEABr can

https://dx.doi.org/10.1021/acsami.0c01173
ACS Appl. Mater. Interfaces 2020, 12, 15928−15933

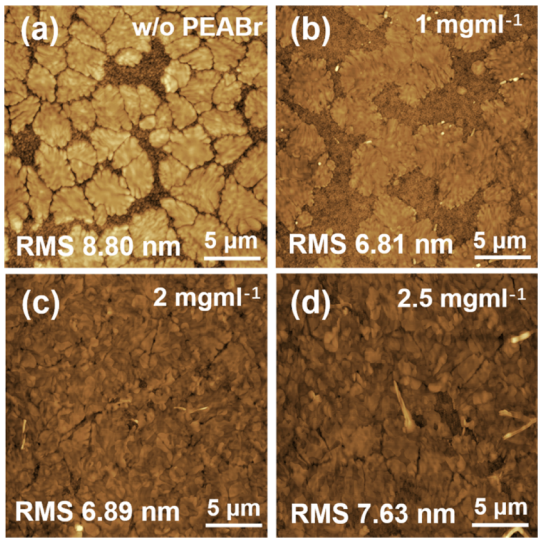

Figure 2. AFM images of perovskite thin films with different concentrations of the PEABr treatment, (a) w/o, (b) 1 mg mL^{-1}, (c) 2 mg mL^{-1}, and (d) 2.5 mg mL^{-1}, respectively.

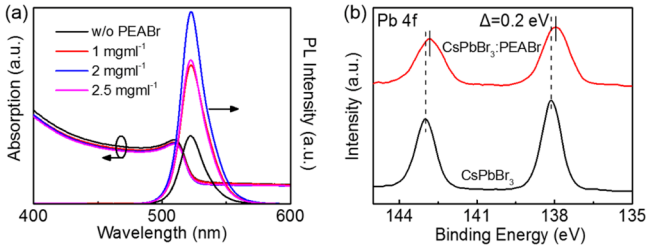

Figure 3. (a) Absorption and the PL spectrum curves for the perovskite films treated with different concentrations of PEABr. (b) Pb 4f core-level spectra for $CsPbBr_3$ and $CsPbBr_3$/PEABr films.

effectively suppress the surface nonradiative defects. Moreover, the PL profile of the perovskite thin films was not affected by PEABr, as shown in Figure S4 (normalized PL). Meanwhile, as shown in Figure S5 and Table S2, after the PEABr treatment, the average lifetime τ_{ave} was prolonged slightly, further verifying the efficient defect-passivation effect of PEABr. To further clarify how PEABr can passivate the defects on the perovskite films, X-ray photoelectron spectroscopy (XPS) was used to examine the chemical states of the PEABr-modified $CsPbBr_3$ films. It can be seen from Figure 3b that after the PEABr treatment, the binding energy of Pb 4f decreased, which is attributed to the increased electron shielding effect on the nucleus of Pb and support PEABr to coordinate with the perovskite surface by sharing electron pairs.[38] It is plausible to conjecture that PEABr would spontaneously assemble quasi-two dimensional perovskite $PEA_2(CsPbBr_3)_{n-1}PbBr_4$ with a larger band gap that passivates the surface defects. Actually, it is extremely tricky to clearly determine whether the quasi-two dimensional perovskite was formed or not because the amount of PEABr is extremely low, as verified by the low N 1s signal (see Figure S6). Nevertheless, the changed chemical states revealed that the PEA^+ was terminated on the $CsPbBr_3$ surface instead of merely being absorbed on it.

To further investigate the impact of PEABr on the performance of the PeLED, modified PeLEDs were fabricated. As seen from the characteristics of $J-V$ in Figure 4a, the current density gradually decreases with the increase of PEABr

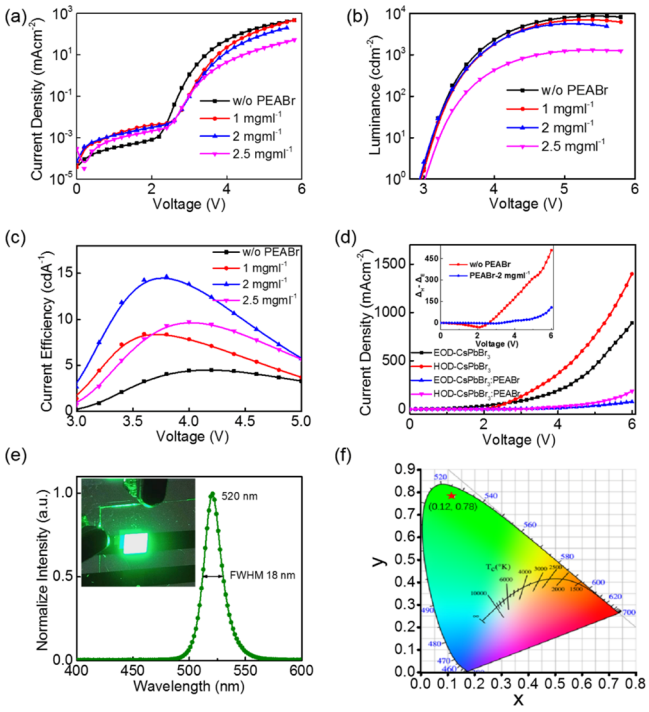

Figure 4. Electrical performance of the PEABr-modified PeLED devices. (a) $J-V$ curves, (b) $L-V$ curves, and (c) CE$-V$ curves of the devices treated with different concentrations of PEABr. (d) Current density of electron/hole-only devices without PEABr and with the PEABr (2 mg mL^{-1}) treatment, the inset is the difference between the current density of the hole-only device (Δ_H) and the current density of the electron-only device (Δ_E) before and after the PEABr treatment. Electron-only device: ITO/LiF (5 nm)/perovskite(with or without PEABr)/LiF (2 nm)/Al; hole-only device: indium tin oxide (ITO)/PEDOT:PSS (40 nm)/perovskite (with or without PEABr)/HAT-CN (10 nm)/Al. (e) EL spectrum with PEABr (2 mg mL^{-1}) treatment, the inset is the picture of device luminescence. (f) CIE color coordinates of the PeLED with PEABr (2 mg mL^{-1}) treatment.

concentration, indicating that PEABr suppresses the carrier transport between the anode and cathode because of the poor conductivity of the large PEA^+ cation. Although the maximum luminance primarily limited by the current density shows a reduction to some extent, the maximum CE and EQE of the devices treated with PEABr (2 mg mL^{-1}) were evidently improved to 14.64 cd A^{-1} and 4.10%, respectively, as shown in Figure 4b,c and Table 1. Such results are the highest current efficiency and EQE for the thermal-evaporation prepared green PeLEDs compared with those reported in the literature.[23,28,29]

The variation in $J-V$ curves as well as the promotion in light-emission efficiency after the PEABr modification demonstrates that PEABr not only passivates the nonradiative traps but also regulates the carrier transport, making a better balance between the holes and the electrons. To elucidate this, hole-only and electron-only devices are constructed (see Figure S7) to investigate whether the electrons and holes injected into the perovskite layer are balanced. As seen from the $J-V$ characteristics in Figure 4d, both the hole and the electron current density are significantly suppressed after the PEABr treatment, which is in line with the electrical properties for the PEABr-modified PeLEDs. For a more intuitive comparison, we plot the difference between the hole and the electron current density, as shown in the inset of Figure 4d. Δ_H

https://dx.doi.org/10.1021/acsami.0c01173
ACS Appl. Mater. Interfaces 2020, 12, 15928−15933

Table 1. Evolution of the Performances (Turn-On Voltage, Maximum Luminance, Maximum CEs, and EQE) for the PeLEDs Treated With Different Concentrations of PEABr

PEABr (mg mL^{-1})	V_{on} (V)	L_{max} (cd m^{-2})	L^a(cd m^{-2})	CE_{max} (cd A^{-1})	CE^a (cd A^{-1})	EQE_{max} (%)
w/o	3.0	8662	8040 ± 476	4.52	4.16 ± 0.21	1.27
1	3.0	7080	7099 ± 765	8.42	8.43 ± 0.64	2.36
2	3.0	5684	4989 ± 747	14.64	13.19 ± 0.42	4.10
2.5	3.0	1310	1028 ± 193	9.75	9.14 ± 0.50	2.73

[a]The values presented are the mean values with their standard deviation (at least 5 samples were examined for each condition).

and Δ_E represent the current density of the hole-only and electron-only device, respectively. Obviously, the PEABr regulation on holes is stronger than that on electrons, indicating that the injected holes and electrons in the PEABr-modified devices are more balanced in contrast to devices without PEABr (because the current density for the hole-only device is larger than that for the electron-only device). Therefore, the improvement in efficiency can be mainly attributed to the following reasons: (i) the enhanced radiative emission by passivating the nonradiative defects via PEABr treatment, and (ii) a more balanced hole and electron transport that resulted in the promotion of recombination efficiency.

Thanks to the stable vacuum preparation condition, the devices exhibited good repeatability, as demonstrated by the performances of 8 separated devices in Table S3. Meanwhile, the stability of these devices has been surveyed under a constant current density. As shown in Figure S8a, the control device without PEABr has a lifetime (T_{50}) of 0.17 h (initial luminance of 100 cd m^{-2}). It is worth noting that the lifetime of our control device is inferior to that reported in the other literatures.[28,29] Thermal degradation caused by joule heat is impossible to be the main reason for this because we carefully scrutinized the PL of the perovskite films under continuous heating at 110 °C and found almost no degradation in 2 h (see Figure S8b). Therefore, we infer that the difference in the device structure between ours and those reported in the literatures may be the origin resulting in the inferior stability of our control device. Encouragingly, the device with a PEABr interface showed an expectedly enhanced stability with T_{50} reaching 0.4 h because of the decreased defects in the perovskite films. The device presents good color purity with an EL peak at 520 nm and a FWHM of 18 nm. The color coordinates of the International Commission on Illumination (CIE) are (0.12, 0.78), as shown in Figure 4e,f, which shows its potential for application in display panels.

CONCLUSIONS

In summary, the efficient PeLEDs with the thermally deposited EML were realized by implementing PEABr as the interfacial modification layer. PEABr terminated on the $CsPbBr_3$ surface, passivated the nonradiative defects, increased the radiative recombination, regulated the charge transport, and consequently significantly improved the optical and electrical performance of PeLEDs. The CE and EQE for the PEABr-modified devices were improved to 14.64 cd A^{-1}, and 4.10%, respectively, at the optimal $CsBr/PbBr_2$ thickness ratio of 9.8:3.2. This work would propose a novel strategy for passivating the defects of the thermally-evaporated perovskite EMLs and provide a helpful guidance for realizing high-performance thermally-evaporated PeLEDs.

EXPERIMENTAL SECTION

Materials. 1,3,5-Tris(*N*-phenylbenzimidazol-2-yl)benzene (TPBi), PEABr (≥99.5%), and PEDOT:PSS (Clevios P AI 4083) were purchased from Xi'an Polymer Light Technology Corp. $PbBr_2$ (99%) was purchased from Macklin. 4,5,8,9,11-Hexaazatriphenylene-hexacarbonitrile (HAT-CN, 99%) and CsBr (99.999%) were purchased from Aldrich. Isopropanol (IPA) was purchased from Infinity Scientific. LiF (99.99%) was purchased from Innochem. All materials were used as received without further purification.

Film and Device Fabrication. The devices were constructed by ITO-coated glass as the anode, PEDOT:PSS as the hole transport layer, thermally deposited perovskite as the emissive layer, TPBi as the electron transport layer, and LiF/Al as the cathode on the top. Prior to device fabrication, the ITO-coated glass substrate was placed in acetone, deionized water, and isopropanol sequentially for ultrasonic cleaning. After drying with nitrogen, the substrate was UV−ozone treated for 15 min. PEDOT:PSS was spin-coated on ITO at 2500 rpm for 40 s and annealed at 140 °C for 10 min in air. The substrate was then transferred to a vacuum chamber (QHV-R20). $PbBr_2$ was deposited by thermal evaporation on the substrate at a rate below 0.4 Å/s with a thickness of 3.2 nm. CsBr was deposited at a rate less than 0.9 Å/s with a desired thickness. Four pairs of $PbBr_2$ and CsBr were successively deposited on the substrates and then annealed at 110 °C for 30 min in an inert atmosphere. PEABr dissolved in IPA was deposited on the perovskite film by spin coating (4500 rpm for 60 s), and annealed at 90 °C for 5 min. Finally, TPBi (40 nm), LiF (2 nm), and Al (100 nm) were sequentially deposited.

Characterization. The UV−vis absorption and PL of perovskite films were acquired by a UV−vis spectrometer (Shimadzu UV-3101PC UV−vis−NIR) and a PL spectrometer (Hitachi fluorescence spectrometer F-7000), respectively. The AFM images of the perovskite films were characterized by Shimadzu SPA-9700. Time-resolved PL decay properties were performed by an Edinburgh FLS920 spectrometer. The thickness of CsBr and $PbBr_2$ were calibrated by a surface profiler ambios XP-1. The XRD patterns were imaged by Bruker D8 Focus. XPS spectra were acquired by Escalab 250Xi. A Keithley 2400 source meter and a luminance meter KONICA MINOLTA LS-160 were used to measure the luminance and the current density of the PeLEDs. The electroluminescence spectrum was measured by an AvaSpec-ULS2048L fiber spectrometer. EQE was calculated based on luminance, current, and EL emission spectrum (assuming Lambertian emission).

ASSOCIATED CONTENT

Supporting Information

The Supporting Information is available free of charge at https://pubs.acs.org/doi/10.1021/acsami.0c01173.

XRD curves; absorption and PL curves; time-resolved PL decay curves; device structure and EL performance of the PeLEDs; electron-only and hole-only device structure; XPS curves; and device stability (PDF)

AUTHOR INFORMATION

Corresponding Authors

Li Song − *Tianjin Key Laboratory of Electronic Materials and Devices, School of Electronics and Information Engineering,*

https://dx.doi.org/10.1021/acsami.0c01173
ACS Appl. Mater. Interfaces 2020, 12, 15928−15933

Hebei University of Technology, Tianjin 300401, P. R. China; orcid.org/0000-0002-4781-4023; Email: songli@hebut.edu.cn

Xingyuan Liu − *State Key Laboratory of Luminescence and Applications, Changchun Institute of Optics, Fine Mechanics and Physics, Chinese Academy of Sciences, Changchun 130033, China;* orcid.org/0000-0002-9681-1646; Email: liuxy@ciomp.ac.cn

Wengang Bi − *Tianjin Key Laboratory of Electronic Materials and Devices, School of Electronics and Information Engineering, Hebei University of Technology, Tianjin 300401, P. R. China;* orcid.org/0000-0002-3231-7980; Email: wbi@hebut.edu.cn

Authors

Kuifeng Jia − *Tianjin Key Laboratory of Electronic Materials and Devices, School of Electronics and Information Engineering, Hebei University of Technology, Tianjin 300401, P. R. China*

Yongsheng Hu − *State Key Laboratory of Luminescence and Applications, Changchun Institute of Optics, Fine Mechanics and Physics, Chinese Academy of Sciences, Changchun 130033, China;* orcid.org/0000-0002-8116-4378

Xiaoyang Guo − *State Key Laboratory of Luminescence and Applications, Changchun Institute of Optics, Fine Mechanics and Physics, Chinese Academy of Sciences, Changchun 130033, China;* orcid.org/0000-0003-0259-137X

Chong Geng − *Tianjin Key Laboratory of Electronic Materials and Devices, School of Electronics and Information Engineering, Hebei University of Technology, Tianjin 300401, P. R. China*

Shu Xu − *Tianjin Key Laboratory of Electronic Materials and Devices, School of Electronics and Information Engineering, Hebei University of Technology, Tianjin 300401, P. R. China;* orcid.org/0000-0002-4185-1392

Ruiting Fan − *Tianjin Key Laboratory of Electronic Materials and Devices, School of Electronics and Information Engineering, Hebei University of Technology, Tianjin 300401, P. R. China*

Lixin Huang − *Tianjin Key Laboratory of Electronic Materials and Devices, School of Electronics and Information Engineering, Hebei University of Technology, Tianjin 300401, P. R. China*

Nannan Luan − *Tianjin Key Laboratory of Electronic Materials and Devices, School of Electronics and Information Engineering, Hebei University of Technology, Tianjin 300401, P. R. China*

Complete contact information is available at: https://pubs.acs.org/10.1021/acsami.0c01173

Notes

The authors declare no competing financial interest.

■ ACKNOWLEDGMENTS

This work was supported by the State Key Laboratory of Luminescence and Applications (no. SKLA-2019-07), the Natural Science Foundation of Hebei Province (nos. F2019202252, F2019202294), the National Natural Science Foundation of China (nos. 61774154, 51672068, 51902082), the Jilin Province Science and Technology Research Project (no. 20180201029GX), and the Natural Science Foundation of Tianjin (no. 17JCYBJC41500).

■ REFERENCES

(1) Wang, N.; Cheng, L.; Ge, R.; Zhang, S.; Miao, Y.; Zou, W.; Yi, C.; Sun, Y.; Cao, Y.; Yang, R.; Wei, Y.; Guo, Q.; Ke, Y.; Yu, M.; Jin, Y.; Liu, Y.; Ding, Q.; Di, D.; Yang, L.; Xing, G.; Tian, H.; Jin, C.; Gao, F.; Friend, R. H.; Wang, J.; Huang, W. Perovskite Light-Emitting Diodes Based on Solution-Processed Self-Organized Multiple Quantum Wells. *Nat. Photonics* **2016**, *10*, 699−704.

(2) Li, M.; Wang, Z.-K.; Yang, Y.-G.; Hu, Y.; Feng, S.-L.; Wang, J.-M.; Gao, X.-Y.; Liao, L.-S. Copper Salts Doped Spiro-Ometad for High-Performance Perovskite Solar Cells. *Adv. Energy Mater.* **2016**, *6*, 1601156.

(3) Fu, Y.; Zhu, H.; Stoumpos, C. C.; Ding, Q.; Wang, J.; Kanatzidis, M. G.; Zhu, X.; Jin, S. Broad Wavelength Tunable Robust Lasing from Single-Crystal Nanowires of Cesium Lead Halide Perovskites ($CsPbX_3$, X = Cl, Br, I). *ACS Nano* **2016**, *10*, 7963−7972.

(4) Wang, Z.-K.; Li, M.; Yang, Y.-G.; Hu, Y.; Ma, H.; Gao, X.-Y.; Liao, L.-S. High Efficiency Pb−In Binary Metal Perovskite Solar Cells. *Adv. Mater.* **2016**, *28*, 6695−6703.

(5) Borchert, J.; Milot, R. L.; Patel, J. B.; Davies, C. L.; Wright, A. D.; Martínez Maestro, L.; Snaith, H. J.; Herz, L. M.; Johnston, M. B. Large-Area, Highly Uniform Evaporated Formamidinium Lead Triiodide Thin Films for Solar Cells. *ACS Energy Lett.* **2017**, *2*, 2799−2804.

(6) Son, D.-Y.; Kim, S.-G.; Seo, J.-Y.; Lee, S.-H.; Shin, H.; Lee, D.; Park, N.-G. Universal Approach toward Hysteresis-Free Perovskite Solar Cell Via Defect Engineering. *J. Am. Chem. Soc.* **2018**, *140*, 1358−1364.

(7) Fang, H.-H.; Wang, F.; Adjokatse, S.; Zhao, N.; Even, J.; Antonietta Loi, M. Photoexcitation Dynamics in Solution-Processed Formamidinium Lead Iodide Perovskite Thin Films for Solar Cell Applications. *Light: Sci. Appl.* **2016**, *5*, No. e16056.

(8) Wei, H.; Fang, Y.; Mulligan, P.; Chuirazzi, W.; Fang, H.-H.; Wang, C.; Ecker, B. R.; Gao, Y.; Loi, M. A.; Cao, L.; Huang, J. Sensitive X-Ray Detectors Made of Methylammonium Lead Tribromide Perovskite Single Crystals. *Nat. Photonics* **2016**, *10*, 333−339.

(9) Xie, C.; You, P.; Liu, Z.; Li, L.; Yan, F. Ultrasensitive Broadband Phototransistors Based on Perovskite/Organic-Semiconductor Vertical Heterojunctions. *Light: Sci. Appl.* **2017**, *6*, No. e17023.

(10) Matsushima, T.; Hwang, S.; Sandanayaka, A. S. D.; Qin, C.; Terakawa, S.; Fujihara, T.; Yahiro, M.; Adachi, C. Solution-Processed Organic−Inorganic Perovskite Field-Effect Transistors with High Hole Mobilities. *Adv. Mater.* **2016**, *28*, 10275−10281.

(11) Shi, Y.; Wu, W.; Dong, H.; Li, G.; Xi, K.; Divitini, G.; Ran, C.; Yuan, F.; Zhang, M.; Jiao, B.; Hou, X.; Wu, Z. A Strategy for Architecture Design of Crystalline Perovskite Light-Emitting Diodes with High Performance. *Adv. Mater.* **2018**, *30*, 1800251.

(12) Zou, Y.; Ban, M.; Yang, Y.; Bai, S.; Wu, C.; Han, Y.; Wu, T.; Tan, Y.; Huang, Q.; Gao, X.; Song, T.; Zhang, Q.; Sun, B. Boosting Perovskite Light-Emitting Diode Performance Via Tailoring Interfacial Contact. *ACS Appl. Mater. Interfaces* **2018**, *10*, 24320−24326.

(13) Tan, Z.-K.; Moghaddam, R. S.; Lai, M. L.; Docampo, P.; Higler, R.; Deschler, F.; Price, M.; Sadhanala, A.; Pazos, L. M.; Credgington, D.; Hanusch, F.; Bein, T.; Snaith, H. J.; Friend, R. H. Bright Light-Emitting Diodes Based on Organometal Halide Perovskite. *Nat. Nanotechnol.* **2014**, *9*, 687−692.

(14) Cao, Y.; Wang, N.; Tian, H.; Guo, J.; Wei, Y.; Chen, H.; Miao, Y.; Zou, W.; Pan, K.; He, Y.; Cao, H.; Ke, Y.; Xu, M.; Wang, Y.; Yang, M.; Du, K.; Fu, Z.; Kong, D.; Dai, D.; Jin, Y.; Li, G.; Li, H.; Peng, Q.; Wang, J.; Huang, W. Perovskite Light-Emitting Diodes Based on Spontaneously Formed Submicrometre-Scale Structures. *Nature* **2018**, *562*, 249−253.

(15) Lin, K.; Xing, J.; Quan, L. N.; de Arquer, F. P. G.; Gong, X.; Lu, J.; Xie, L.; Zhao, W.; Zhang, D.; Yan, C.; Li, W.; Liu, X.; Lu, Y.; Kirman, J.; Sargent, E. H.; Xiong, Q.; Wei, Z. Perovskite Light-Emitting Diodes with External Quantum Efficiency Exceeding 20 Percent. *Nature* **2018**, *562*, 245−248.

(16) Chiba, T.; Hayashi, Y.; Ebe, H.; Hoshi, K.; Sato, J.; Sato, S.; Pu, Y.-J.; Ohisa, S.; Kido, J. Anion-Exchange Red Perovskite Quantum Dots with Ammonium Iodine Salts for Highly Efficient Light-Emitting Devices. *Nat. Photonics* **2018**, *12*, 681−687.

(17) Shi, Z.; Li, S.; Li, Y.; Ji, H.; Li, X.; Wu, D.; Xu, T.; Chen, Y.; Tian, Y.; Zhang, Y.; Shan, C.; Du, G. Strategy of Solution-Processed All-Inorganic Heterostructure for Humidity/Temperature-Stable Per-

ovskite Quantum Dot Light-Emitting Diodes. *ACS Nano* **2018**, *12*, 1462−1472.
(18) Cai, W.; Chen, Z.; Li, Z.; Yan, L.; Zhang, D.; Liu, L.; Xu, Q.-h.; Ma, Y.; Huang, F.; Yip, H.-L.; Cao, Y. Polymer-Assisted in Situ Growth of All-Inorganic Perovskite Nanocrystal Film for Efficient and Stable Pure-Red Light-Emitting Devices. *ACS Appl. Mater. Interfaces* **2018**, *10*, 42564−42572.
(19) Jin, F.; Zhao, B.; Chu, B.; Zhao, H.; Su, Z.; Li, W.; Zhu, F. Morphology Control Towards Bright and Stable Inorganic Halide Perovskite Light-Emitting Diodes. *J. Mater. Chem. C* **2018**, *6*, 1573−1578.
(20) Rakita, Y.; Kedem, N.; Gupta, S.; Sadhanala, A.; Kalchenko, V.; Böhm, M. L.; Kulbak, M.; Friend, R. H.; Cahen, D.; Hodes, G. Low-Temperature Solution-Grown $CsPbBr_3$ Single Crystals and Their Characterization. *Cryst. Growth Des.* **2016**, *16*, 5717−5725.
(21) El Ajjouri, Y.; Palazon, F.; Sessolo, M.; Bolink, H. J. Single-Source Vacuum Deposition of Mechanosynthesized Inorganic Halide Perovskites. *Chem. Mater.* **2018**, *30*, 7423−7427.
(22) Lin, H. Y.; Chen, C. Y.; Hsu, B. W.; Cheng, Y. L.; Tsai, W. L.; Huang, Y. C.; Tsao, C. S.; Lin, H. W. Efficient Cesium Lead Halide Perovskite Solar Cells through Alternative Thousand-Layer Rapid Deposition. *Adv. Funct. Mater.* **2019**, *29*, 1905163.
(23) Li, J.; Du, P.; Li, S.; Liu, J.; Zhu, M.; Tan, Z.; Hu, M.; Luo, J.; Guo, D.; Ma, L.; Nie, Z.; Ma, Y.; Gao, L.; Niu, G.; Tang, J. High-Throughput Combinatorial Optimizations of Perovskite Light-Emitting Diodes Based on All-Vacuum Deposition. *Adv. Funct. Mater.* **2019**, *29*, 1903607.
(24) Jang, J.; Choe, G.; Yim, S. Effective Control of Chlorine Contents in $MAPbI_{3-x}Cl_x$ Perovskite Solar Cells Using a Single-Source Vapor Deposition and Anion-Exchange Technique. *ACS Appl. Mater. Interfaces* **2019**, *11*, 20073−20081.
(25) Longo, G.; Momblona, C.; La-Placa, M.-G.; Gil-Escrig, L.; Sessolo, M.; Bolink, H. J. Fully Vacuum-Processed Wide Band Gap Mixed-Halide Perovskite Solar Cells. *ACS Energy Lett.* **2018**, *3*, 214−219.
(26) Gil-Escrig, L.; Momblona, C.; La-Placa, M.-G.; Boix, P. P.; Sessolo, M.; Bolink, H. J. Vacuum Deposited Triple-Cation Mixed-Halide Perovskite Solar Cells. *Adv. Energy Mater.* **2018**, *8*, 1703506.
(27) Jiang, Q.; Zhao, Y.; Zhang, X.; Yang, X.; Chen, Y.; Chu, Z.; Ye, Q.; Li, X.; Yin, Z.; You, J. Surface Passivation of Perovskite Film for Efficient Solar Cells. *Nat. Photonics* **2019**, *13*, 460−466.
(28) Hu, Y.; Wang, Q.; Shi, Y.-L.; Li, M.; Zhang, L.; Wang, Z.-K.; Liao, L.-S. Vacuum-Evaporated All-Inorganic Cesium Lead Bromine Perovskites for High-Performance Light-Emitting Diodes. *J. Mater. Chem. C* **2017**, *5*, 8144−8149.
(29) Lian, X.; Wang, X.; Ling, Y.; Lochner, E.; Tan, L.; Zhou, Y.; Ma, B.; Hanson, K.; Gao, H. Light Emitting Diodes Based on Inorganic Composite Halide Perovskites. *Adv. Funct. Mater.* **2018**, *29*, 1807345.
(30) Zhang, X.; Lin, H.; Huang, H.; Reckmeier, C.; Zhang, Y.; Choy, W. C. H.; Rogach, A. L. Enhancing the Brightness of Cesium Lead Halide Perovskite Nanocrystal Based Green Light-Emitting Devices through the Interface Engineering with Perfluorinated Ionomer. *Nano Lett.* **2016**, *16*, 1415−1420.
(31) Bi, W.; Cui, Q.; Jia, P.; Huang, X.; Zhong, Y.; Wu, D.; Tang, Y.; Shen, S.; Hu, Y.; Lou, Z.; Teng, F.; Liu, X.; Hou, Y. Efficient Quasi-Two-Dimensional Perovskite Light-Emitting Diodes with Improved Multiple Quantum Well Structure. *ACS Appl. Mater. Interfaces* **2020**, *12*, 1721−1727.
(32) Wang, Y.; Zhang, T.; Kan, M.; Li, Y.; Wang, T.; Zhao, Y. Efficient α-$CsPbI_3$ Photovoltaics with Surface Terminated Organic Cations. *Joule* **2018**, *2*, 2065−2075.
(33) Song, L.; Guo, X.; Hu, Y.; Lv, Y.; Lin, J.; Fan, Y.; Zhang, N.; Liu, X. Improved Performance of $CsPbBr_3$ Perovskite Light-Emitting Devices by Both Boundary and Interface Defects Passivation. *Nanoscale* **2018**, *10*, 18315−18322.
(34) Liu, X.; Guo, X.; Lv, Y.; Hu, Y.; Fan, Y.; Lin, J.; Liu, X.; Liu, X. High Brightness and Enhanced Stability of $CsPbBr_3$-Based Perovskite Light-Emitting Diodes by Morphology and Interface Engineering. *Adv. Opt. Mater.* **2018**, *6*, 1801245.
(35) Wang, Z.; Wang, F.; Sun, W.; Ni, R.; Hu, S.; Liu, J.; Zhang, B.; Alsaed, A.; Hayat, T.; Tan, Z. a. Manipulating the Trade-Off between Quantum Yield and Electrical Conductivity for High-Brightness Quasi-2D Perovskite Light-Emitting Diodes. *Adv. Funct. Mater.* **2018**, *28*, 1804187.
(36) Ling, Y.; Tan, L.; Wang, X.; Zhou, Y.; Xin, Y.; Ma, B.; Hanson, K.; Gao, H. Composite Perovskites of Cesium Lead Bromide for Optimized Photoluminescence. *J. Phys. Chem. Lett.* **2017**, *8*, 3266−3271.
(37) Zhang, H.; Ye, F.; Li, W.; Yao, J.; Gurney, R. S.; Liu, D.; Xiong, C.; Wang, T. Bright Perovskite Light-Emitting Diodes with Improved Film Morphology and Reduced Trap Density Via Surface Passivation Using Quaternary Ammonium Salts. *Org. Electron.* **2019**, *67*, 187−193.
(38) Huang, G.; Wang, C.; Zhang, H.; Xu, S.; Xu, Q.; Cui, Y. Post-Healing of Defects: An Alternative Way for Passivation of Carbon-Based Mesoscopic Perovskite Solar Cells Via Hydrophobic Ligand Coordination. *J. Mater. Chem. A* **2018**, *6*, 2449−2455.

https://dx.doi.org/10.1021/acsami.0c01173
ACS Appl. Mater. Interfaces 2020, 12, 15928−15933